Molecular Therapy
Nucleic Acids
Original Article

Targeting heterozygous dominant negative variant of *KCNA2* using Gapmer ASO for the treatment of drug-resistant epilepsy

Hua Huang,[1,2,3,4,5] Dong Rui Ma,[6,7] Derrick Wei Shih Chan,[8] Adeline Seow Fen Ngoh,[8] Dejie Yu,[2] Shi Jun Ng,[1] John Jia En Chua,[1,3,4] Eng King Tan,[11,12] Hui-Lin Chin,[9,10] Denise Li Meng Goh,[9,10] and Tuck Wah Soong[1,3,4,5]

[1]Department of Physiology, Yong Loo Lin School of Medicine, National University of Singapore, Singapore 117597, Singapore; [2]Electrophysiology Core Facility, Yong Loo Lin School of Medicine, National University of Singapore, Singapore 117544, Singapore; [3]LSI Neurobiology Programme, National University of Singapore, Singapore 117456, Singapore; [4]Healthy Longevity Translational Research Program, Yong Loo Lin School of Medicine, National University of Singapore: Level 5, Centre for Life Sciences, 28 Medical Drive, Singapore 117456, Singapore; [5]Cardiovascular-Metabolic Disease Translational Research Programme, National University of Singapore, 14 Medical Drive, MD6, #08-01, Singapore 117599, Singapore; [6]Department of Neurology, Singapore General Hospital, Singapore 169856, Singapore; [7]DUKE-NUS Medical School, Singapore 169857, Singapore; [8]Paediatric Neurology, KK Women's and Children's Hospital, 100 Bukit Timah Road, Singapore 229899, Singapore; [9]Department of Paediatrics, Khoo Teck Puat - National University Children's Medical Institute, National University Hospital, National University Health System, Singapore, Singapore; [10]Department of Paediatrics, Yong Loo Lin School of Medicine, National University of Singapore, Singapore, Singapore; [11]Neuroscience and Behavioral Disorder, DUKE-NUS Medical School, Singapore 169857, Singapore; [12]National Neuroscience Institute, Department of Neurology, Singapore 308433, Singapore

A missense mutation c.1220C>G of *KCN2A* gene was recently identified in an infant with epilepsy. *KCNA2* encodes K_V1.2 subunits that form voltage-gated potassium channels (VGKC) via tetrameric assembly. The mutation results in amino acid change P407R at the highly conserved *PVP* motif. Functional characterization revealed that mutant K_V1.2_P407R subunits formed loss-of-function channels and suppressed both K_V1.2 and K_V1.1 channel activities. Hetero-tetrameric assembly of the K_V1.2_P407R subunits with other neuronal voltage-gated potassium channels of Shaker subfamily could lead to general deficit of repolarizing potassium current and potentially underlie the enhanced seizure susceptibility. Indeed, expression of human K_V1.2_P407R in early postnatal rat cortical neurons or genetically engineered hESC-derived neurons disclosed broadening of action potential duration and early afterdepolarization (EAD), associating with reduced potassium current. We hypothesize that Gapmer antisense oligonucleotides (ASOs) targeted to c.1220C>G mutation will selectively degrade the mutant mRNA while allowing the remaining wild-type (WT) subunits to form functional channels. As a proof of principle, delivery of Gapmer packaged in lipid nanoparticle into cortical neurons selectively suppressed K_V1.2_P407R over the WT protein expression, reversing the broadening of action potential duration, abrogating the EAD and leading to overall increase in potassium current.

INTRODUCTION

Epilepsy is a neurological disorder that is characterized by recurring, abnormal brain activity causing seizures or periods of unusual behavior, sensations, and sometimes loss of awareness. Monogenic variations account for 40% of cases with severe epilepsy.[1] Channelopathies, particularly those involving voltage-gated sodium and potassium channel genes, are responsible for a variety of epilepsy syndromes among other neurological diseases.

Recently, an epilepsy gene panel in an infant with epilepsy revealed a previously uncharacterized missense mutation in *KCNA2*, which encodes voltage-gated potassium channel (VGKC) K_V1.2. The proband was the first child of non-consanguineous healthy parents. She presented in early infancy with unprovoked generalized seizures. Brain magnetic resonance imaging did not reveal any abnormalities. Electroencephalogram showed spikes and sharp waves over the right hemisphere and left posterior temporal region. She had multiple generalized seizures and several episodes of status epilepticus. Her seizures were difficult to control despite the use of multiple medications. She was initially treated with carbamazepine, but this was ineffective due to auto-induction. Seizure control subsequently improved on a combination of levetiracetam, phenytoin, and sodium valproate. When a resurgence in seizures occurred, oxcarbazepine was added with brief improvement. She developed further seizures and had transaminitis and hyperammonemia, secondary to sodium valproate. Zonisamide was added to her treatment. Apart of epilepsy, she also had esotropia and global developmental delay. Presently at the age of 4 years, she speaks mostly in single words and is in special education. She is hypotonic and has both truncal and peripheral ataxia. She is unable to mobilize independently.

Received 13 June 2024; accepted 23 August 2024;
https://doi.org/10.1016/j.omtn.2024.102316.

Correspondence: Hua Huang, Department of Physiology, Yong Loo Lin School of Medicine, National University of Singapore, Singapore 117597, Singapore.
E-mail: phshhua@nus.edu.sg

Table 1. In silico predictions for *KCNA2* c.1220C>G; p.(Pro407Arg) performed with Alamut Visual Plus, SOPHiA Genetics

gnomAD, 1000G, ESP	dbSNP	SIFT	GVGD	Mutation taster	PolyPhen	CADD
Absent	No entry	DEL (score: 0.00, median: 4.32)	Class C0 (GV: 208.63 - GD: 101.15)	Deleterious. Tree vote: 93|7 (del|benign).	HDivPred: probably damaging (score: 1). HVarPred: probably damaging (score: 1)	26.7

1000G, 1000 Genomes; CADD, Combined Annotation Dependent Depletion; Del, deleterious; GVGD, Grantham variation Grantham distance.

Genetic testing via an epilepsy gene panel was performed soon after her first presentation. It revealed that she was heterozygous for a likely pathogenic variant, *KCNA2* (NM_004974.3:c.1220C>G); p.(Pro407Arg)) classified by the laboratory as a "likely pathogenic" variant per the ACMG-AMP 2015 guidelines.[2] This variant is not present in population databases (gnomAD, ExAC, 1000G) (PM2). This is a missense variant in a gene that has a low rate of benign missense variation, and missense variants are a common mechanism of disease (PP2). The sequence change replaces proline, which is neutral and non-polar, with arginine, which is basic and polar, at codon 407 of the K_V1.2 protein (p.Pro407Arg). The Grantham matrix score of this variant is 103. Multiple lines of computational evidence support a deleterious effect on the gene (Table 1) (PP3). Another variant p.(Pro407Ala) that disrupts this p.Pro407 residue has been determined to be pathogenic (PM5)[3]; it was identified in a 3-year-old girl with neonatal-onset epileptic encephalopathy and profound intellectual disability. Clinvar has an entry for this variant (1067683). Parental segregation was checked via Sanger sequencing provided commercially (www.invitae.com) and confirmed this variant occurred *de novo* (PM6). The proband's phenotype was concordant with previous descriptions of individuals with *KCNA2*-related infantile epileptic encephalopathy.

Voltage-gated potassium channels form membrane aqueous conduits to facilitate the outflux of the positively charged K^+ ion and thereby serve to dampen neuronal excitability. Among the Shaker subfamily of voltage-gated potassium channels, K_V1.1, K_V1.2, and K_V1.4 are most abundantly expressed in the brain. While K_V1.1 knockout (KO) mice show limbic seizure phenotypes similar to that of temporal lobe epilepsy, K_V1.2 KO mice have more severe brainstem seizure phenotypes and die before postnatal day 19.[4,5] In comparison, K_V1.4 KO mice only exhibit mild hyperactivity.[6] K_V1.1 and 1.2 channels, localized at the axon initial segment (AIS), play an important role in regulating action potential (AP) initiation and frequency. Enrichment of such channels at the juxtaparanodal regions in the axon serve to quickly repolarize the axon and support rapid conduction of AP.[5] Inhibition of both K_V1.1 and K_V1.2 channels with α-dendrodotoxin (DTX-alpha) leads to increased spontaneous firing frequency.[7] Adding to the complexity, K_V1.1 and K_V1.2 channel subunits have been reported to form hetero-tetramers with different pharmacological sensitivities.[8]

Subsequent patch-clamp electrophysiological characterization in transfected HEK293FT cells revealed that K_V1.2_P407R subunits form loss-of-function channels. Upon co-expression with the K_V1.2_WT and K_V1.1 channel subunits, the K_V1.2_P407R variant almost completely suppressed K_V1.2 channel activities while partially affecting the K_V1.1 current. Given the hetero-tetrameric assembly of the K_V1.2_P407R variant with K_V1.2_WT and potentially with other neuronal voltage-gated potassium channels of the Shaker subfamily, such heterozygous dominant negative variants could potentially lead to a deficit of overall voltage-gated potassium conductance in neurons and underlie the pathogenesis of recurrent afebrile seizures at early infancy. Indeed, overexpression of human K_V1.2_P407R in early postnatal rat cortical neurons disclosed broadening of AP duration and early afterdepolarization (EAD) as compared with K_V1.2_WT expressing or control neurons, associating with reduced repolarizing potassium current. Genome-edited human induced pluripotent stem cell derived neurons (hESC-derived neuron) expressing K_V1.2_P407R displayed similar EAD pattern and reduction in the potassium current.

As potassium channels are complexes assembled from four similar subunits, hetero-tetrameric assembly of subunits of different subtypes within Shaker channels could result in channels of mixed biophysical and pharmacological properties.[9] This poses significant challenges to successfully design a single small molecular channel modulator to rescue individual hetero-tetrameric complexes that contain Kv1.2_P407R subunits. To circumvent the abovementioned problems of targeting channel proteins, we have designed and tested Gapmer antisense oligonucleotides (ASOs) targeted to c.1220C>G mutation. Presumably, selective degradation of the mutant mRNA inhibits the protein production of K_V1.2_P407R subunits, while the remaining wild-type (WT) subunits could still assemble to form functional channels.

ASOs are short, synthetic DNA molecules that bind to target RNA via Watson-Crick base pairing to mediate a range of gene regulatory mechanisms from transcript cleavage and degradation, splice switching to translational repression or activation. ASOs could be broadly divided into steric block or RNase H competent. Masking of splicing factor binding by steric block ASOs leads to splice switching and provides a mechanistic basis for the development of therapeutics such as Eteplirsen and Nusinersen, which were approved by the Food and Drug Administration (FDA) for the treatment of Duchenne muscular dystrophy and spinal muscular atrophy, respectively.[10]

While steric block ASOs contain modifications such as 2′-O-Methoxyethyl (2′-MOE) or 2′-O-methyl in the ribose sugar moiety that do not activate RNase H, Gapmer ASOs on the other hand are special

ASOs that comprise a central "gap" region of unmodified DNA flanked by 2′-MOE modified DNA. Binding of unmodified DNA to RNA activates RNase H-mediated degradation of the complementary RNA, resulting in gene product reduction. 2′-MOE modifications confer enhanced nuclease resistance, lower toxicity, and increased hybridization affinities. Additional stability and base-pairing specificity could be afforded by including locked nucleic acid (LNA) containing a methylene bridge bond between the 2′ oxygen and the 4′ carbon of the pentose ring. Such conformation reportedly enhances base stacking perfectly matched base pairs and decrease stabilizing stacking interactions of mismatched base pairs therefore contributing to higher potency and specificity of Gapmer ASOs.[11–13] The internucleotide (phosphodiester) bonds could be replaced with phosphorothioate (PS) linkages to further increase nuclease resistance. Gapmers such as Mipomersen and Inotersen have been approved by the FDA for the treatment of homozygous familial hypercholesterolemia and polyneuropathy due to hereditary transthyretin amyloidosis, respectively. A Gapmer targeting the sodium channel gene *SCN1A* is currently undergoing clinical trial for rare, drug-resistant epilepsies.[10]

In the current study, co-transfection of c.1220C>G targeting Gapmer#3, K_V1.2_WT and P407R subunits revealed selective down-regulation of K_V1.2_P407R over WT protein and significantly rescued K_V1.2 and K_V1.1 current density in transfected HEK293FT cells. As a proof of principle for further clinical application, delivery of Gapmer#3 packaged in lipid nanoparticle (LNP) to cortical neurons was shown to selectively suppress K_V1.2_P407R expression over the WT protein. Gapmer#3 reversed the broadening of AP, abrogating the EAD and led to overall increase in potassium current in K_V1.2_P407R expressing neurons. The result and methodology discussed in the current study not only support the development of a novel personalized therapy for our patient harboring the c.1220C>G *KCN2A* variant but can potentially be applied to design similar therapeutics for other *KCNA2* dominant mutations.

RESULTS

The missense *KCNA2* mutation c.1220C>G yields dominant negative K_V1.2_P407R subunits

The channel complexes of voltage-gated potassium channels are assembled from four identical subunits. Each subunit consists of six transmembrane helixes. The domain comprising S1 to S4 helixes function as voltage-sensing domain and S5 and S6 helix and the membrane re-entrant loop in-between them is the pore-forming domain. *In silico* translation predicts c.1220C>G results in amino acid change in P407R in the S6 segment closer to the intracellular face (uniprot: p16389, https://www.uniprot.org/uniprotkb/P16389/entry) (Figure 1A). The two proline residues in the *PVP* motif are highly conserved among vertebrates as revealed by sequence alignment data in the ENCODE database (Figure 1B). The mutation affects the second proline residue in the highly conserved *PVP* motif that functions as a flexible hinge to allow for electro-mechanical coupling between the voltage-sensing domain and the opening of intracellular gates (Figure 1C).[14,15] To enable functional characterization of the impact of the P407R change, the coding sequence of K_V1.2_WT was cloned and subsequently in the same sequence the c.1220C>G mutation was generated by circular mutagenesis (Figure 1D). A hemagglutinin (HA) tag was engineered before the stop codon to facilitate the detection of the K_V1.2 protein by western blot. Subsequent surface biotinylation assay revealed comparable expression levels of K_V1.2_WT and K_V1.2_P407R proteins in both whole-cell lysate and surface fraction indicating that P407R amino acid change did not affect protein expression or surface trafficking of K_V1.2 channels (Figure 1E).

Expression of K_V1.2_WT in HEK293FT cells yielded robust outward voltage-gated potassium current with peak current density of 1934.0 + 271.7 pA/pF at 50 mV (Figure 2A). In comparison, little current was observed upon expression of K_V1.2_P407R with peak current density of 21.18 + 2.57 pA/pF (Figures 2B and 2D). Significantly, co-expression of the K_V1.2_WT and K_V1.2_P407R also resulted in very little channel activities with peak current density of 52.57 + 8.37 pA/pF (Figures 2C and 2D), suggesting that K_V1.2_P407R was not only inactive on its own but could also exert dominant negative effect over the WT channel. The K_V1.2_WT and K_V1.2_P407R coding sequences (cds) were subcloned into the expression vectors pIRES2-DsRed and pIRES2-EGFP, respectively, to allow for identification by co-expression of reporter fluorescent proteins. The expression of red dsRed and green EGFP allows for visual identification of cells expressing either WT or P407R mutant proteins, respectively. Only yellow cells were picked for patch-clamp characterization in the co-transfection experiment (Figure S1).

In addition, K_V1.1 and K_V1.2 channel subunits reportedly form hetero-tetramers.[8] To test if the dominant negative effect of K_V1.2_P407R could also affect K_V1.1 channel function, we co-expressed K_V1.1 with K_V1.2_WT or K_V1.2_P407R. While the K_V1.2_WT did not significantly affect the peak current density of K_V1.1 channels (Figures 2D and 2E), co-transfection of K_V1.2_P407R with K_V1.1 yielded significantly less peak current density (1233.5 ± 193.9 pA/pF) as compared with K_V1.1 expressing cells (3035.9 ± 503.1 pA/pF) or K_V1.2_WT and K_V1.1 co-expressing cells (3248.5 ± 533.8 pA/pF) (Figures 2E and 2F), suggesting that K_V1.2_P407R can have far-reaching consequences affecting other Shaker channel activities in neurons. Supportingly, subsequent co-immunoprecipiation detected robust interaction between K_V1.2_P407R and K_V1.2_WT, K_V1.2_WT and K_V1.1 and K_V1.2_P407R and K_V1.1 subunits, indicating that Kv1.2_P407R affects the activity of K_V1.2_WT and K_V1.1 potentially via formation of hetero-tetrameric channel complexes (Figure S2).

c.1220C>G mutation-specific Gapmer#3 selectively downregulates the expression of K_V1.2_P407R protein

Given that K_V1.2_P407R subunits assembles into hetero-tetrameric channel complexes with K_V1.2_WT and K_V1.1 subunits with random permutations, it would be challenging to successfully design single small molecular channel modulators to overcome the suppressive effect of K_V1.2_P407R on all possible heteromeric channel complexes. As an alternative to directly targeting channel proteins, we designed and tested Gapmer ASOs targeted to c.1220C>G mutation as an attempt to selectively degrade the mutant mRNA over WT transcripts. To

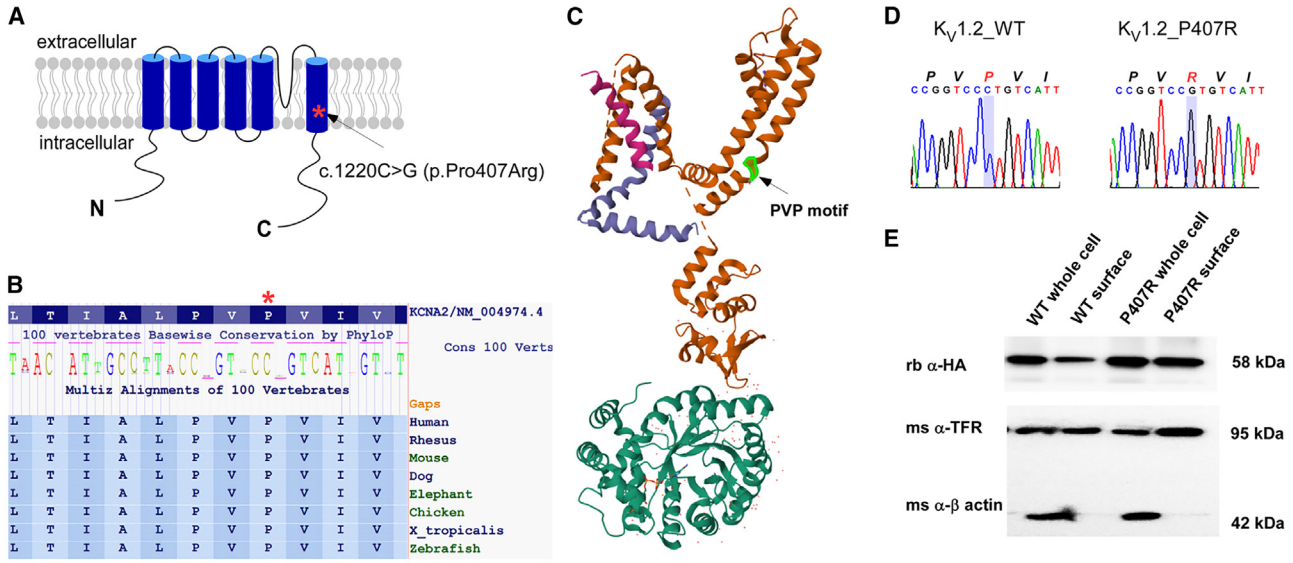

Figure 1. Expression of K_V1.2 _WT and K_V1.2 _P407R in transfected HEK293FT cells

(A) Topology of a single K_V1.2 subunit. The asterisk indicates the position of P407R change. (B) Alignment of coding sequence of partial S6 segment of K_V1.2 showing high conservation of the *PVP* motif; the P407 residue is highlighted by an asterisk. (C) Structure of mammalian Shaker K_V1.2 potassium channel-beta subunit complex. The *PVP* motif is highlighted in green. Only one K_V1.2 subunit and one beta subunit are shown.[16] (D) DNA sequencing confirmation of cloning of K_V1.2_WT and K_V1.2_P407R. (E) Surface biotinylation experiment revealed comparable expression level and surface trafficking of K_V1.2 _WT and K_V1.2 _P407R protein. TFR was used as a surface marker and β-actin as the cytosolic marker.

this end, a 15-nucleotide (nt) ASO was designed containing a mix of 2′-MOE modified nucleotides and LNAs at the 5′ and 3′ end and a central "gap" region containing unmodified nucleotides. The internucleotide (phosphodiester) bonds were replaced with phosphorothioate (PS) linkages to further increase nuclease resistance (Figure 3A). The Gibbs free energy as predicted with RNA structure 6.0 software[17] was lower for the transcript containing c.1220C>G (−28.9 kJ/mol) as compared with the WT (−23.1 kJ/mol), suggesting higher affinity of Gapmer#3 to the mutant transcript, thus allowing it to preferentially target mutant over WT mRNA. Conformingly, in cells co-expressing HA-tagged K_V1.2_WT and Flag (FL)-tagged K_V1.2_P407R proteins, co-transfection of increasing doses of Gapmer#3 led to progressive down-regulation of K_V1.2_P407R protein specifically (Figure 3B). Subsequent densitometry analysis showed that Gapmer#3 inhibited the expression of K_V1.2_P407R with IC_{50} = 1.09 nM while the IC_{50} value for K_V1.2_WT could not be determined. Correlatingly, the peak current density of K_V1.2_WT and K_V1.2_P407R expressing cells increased significantly from 52.57 + 8.37 pA/pF to 993.3 ± 173.5 pA/pF upon co-transfected of 2.5 nM Gapmer#3 and the peak current density of K_V1.1 and K_V1.2_P407R expressing cells also increased significantly from 1233.5 ± 193.9 pA/pF to 3124.1 ± 521.2 pA/pF (Figures 3C and 3D).

Expression of K_V1.2_P407R protein is associated with broadening of AP and early afterdepolarization (EAD) in rat cortical neurons and hESC-derived neurons

K_V1.1 and K_V1.2 channels characteristically activate at low voltage threshold and play critical roles in modulating AP duration and kinetics.[18] To understand the physiological impact of c.1220C>G mutation, rat cortical neurons were cultured from postnatal day 0 rat pups and 1 day after plating, the neurons were transduced with Lentivirus expressing HA-tagged K_V1.2_WT or K_V1.2_P407R and downstream EGFP sequence via an internal ribosomal entry sequence (IRES). Neurons that expressed only the EGFP protein were used as control. Robust EGFP fluorescent signals were observed 10 days after viral transduction (Figure S3A). RT-PCR identified neurons expressing either K_V1.2_WT or K_V1.2_P407R based on the c.1220C>G difference while two silent nucleotide differences flanking c.1220C>G differentiate endogenous rat K_V1.2 transcripts in control neurons from the neurons expressing human K_V1.2 transcripts (Figure S3B). Moreover, western blot analysis of the cell lysate revealed the expression of HA-tagged exogenous K_V1.2_WT and Kv1.2_P407R proteins only in the WT and P407R expressing cells but not in the control cells. The expression of endogenous K_V1.1 channel was not substantially affected by the expression of K_V1.2_WT or K_V1.2_P407R protein. Last, α-K_V1.2 antibody confirmed the overexpression of K_V1.2_WT and K_V1.2_P407R in transduced cells compared with endogenous K_V1.2 in control cells (Figure S3C).

The transduced neurons were subjected to patch-clamp analysis 7 days post viral transduction. The neurons displayed robust AP firing upon injection of positive current. Intriguingly, dramatic EAD, which manifested as secondary voltage depolarizations during the repolarizing phase of the AP, were commonly observed among P407R neurons, in stark contrast to the solitary spikes observed in control or WT neurons (Figures S4A–S4C). Blockade

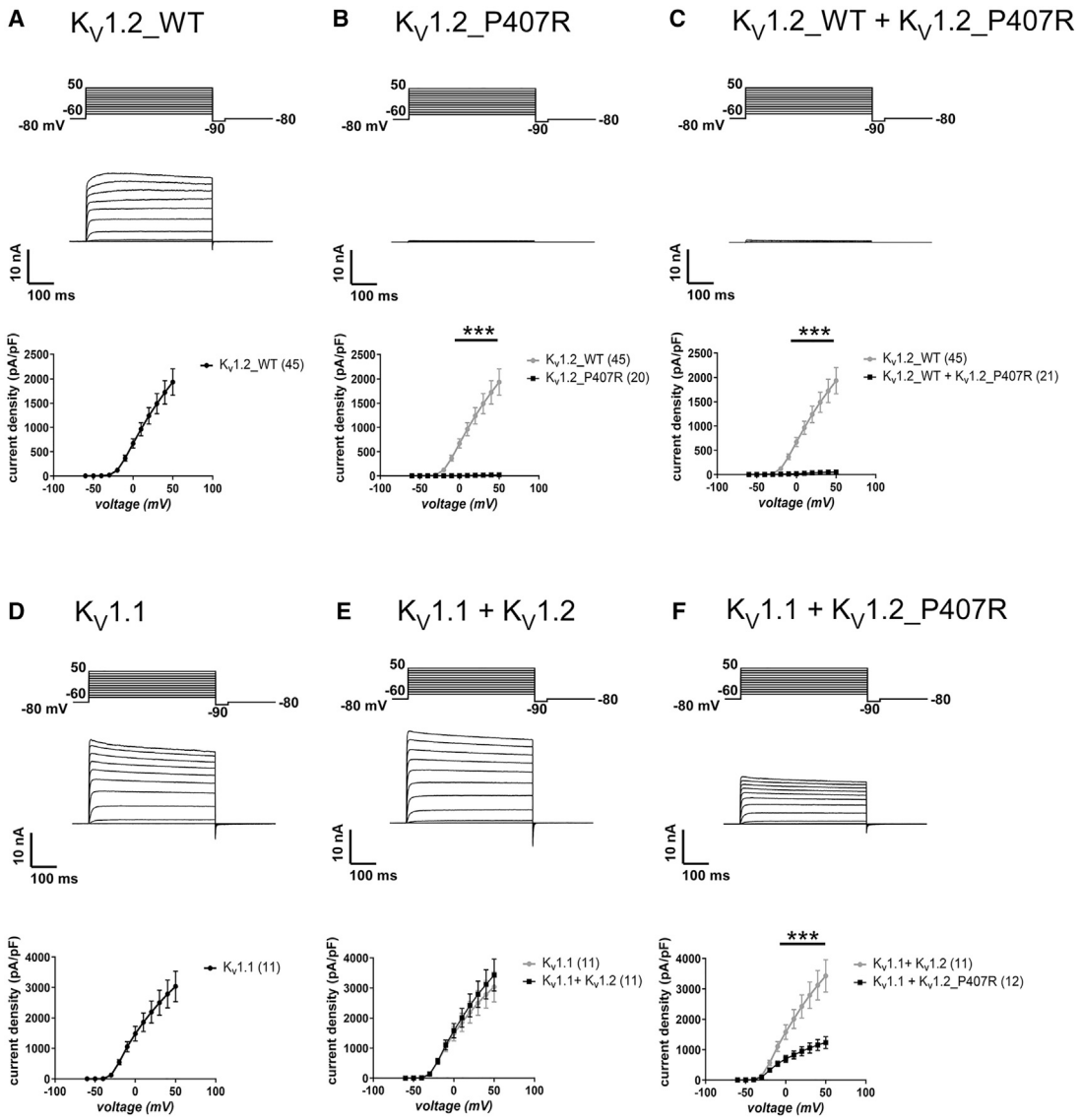

Figure 2. K_V1.2_P407R inhibits the K_V1.2 and K_V1.1 currents in a dominant negative manner

(A) Top, schematic of voltage stimuli. Briefly, K_V1.2 and K_V1.1 currents were evoked from holding potential of −80 mV to different test potentials ranging from −60 mV to 50 mV. The tail currents were evoked subsequently upon returning the voltage to −90 mV. Middle, exemplary K_V1.2_WT currents. Bottom, current density-voltage profile of K_V1.2_WT current. The current densities were obtained by normalizing the whole cell current (pA) over the cell capacitance (pF). The number of cells recorded is indicated by the numbers in parentheses. (B) Effect of P407R mutation on K_V1.2 channel function, format as in (A). The profile of K_V1.2_WT currents is reproduced from (A) for comparison. (C) Effect of K_V1.2_P407R on K_V1.2_WT function upon co-transfection, format as in (B). (D) Characterization of cells transfected with K_V1.1 channel, format as in (A). (E) Currents observed in cells co-expressing both K_V1.1 and K_V1.2_WT, format as in (A). The profile of K_V1.1 current is reproduced from (D) for comparison. (F) Effect of K_V1.2_P407R on K_V1.1 function upon co-transfection, format as in (B). The profile of K_V1.1+ K_V1.2 current is reproduced from (E) for comparison. ***$p < 0.001$ The data presented are mean ± SEM. Statistical significance was tested using unpaired Student's t test (2-tails).

of KCNQ/M potassium channel with linopirdine and XE991 has been shown to enhance the spike after depolarization converting single AP spikes into a burst firing of multiple spikes in hippocampal neurons.[19] Similarly blockade of K_V1.1 and K_V1.2 by dendrotoxin lead to EAD in CA1 hippocampal neuron.[20] To quantify and compare the kinetics of APs, the amplitude of APs is defined as the voltage difference between the peak and trough of the AP. The half action potential duration APD_{50} was measured at the half action potential amplitude and the extent of EAD was quantified by the AP area under the curve between 10 ms before AP peak and the trough (Figure S4D).

Analysis of the first AP evoked by current injection was subsequently performed. Curiously, AP area was significantly larger in P407R

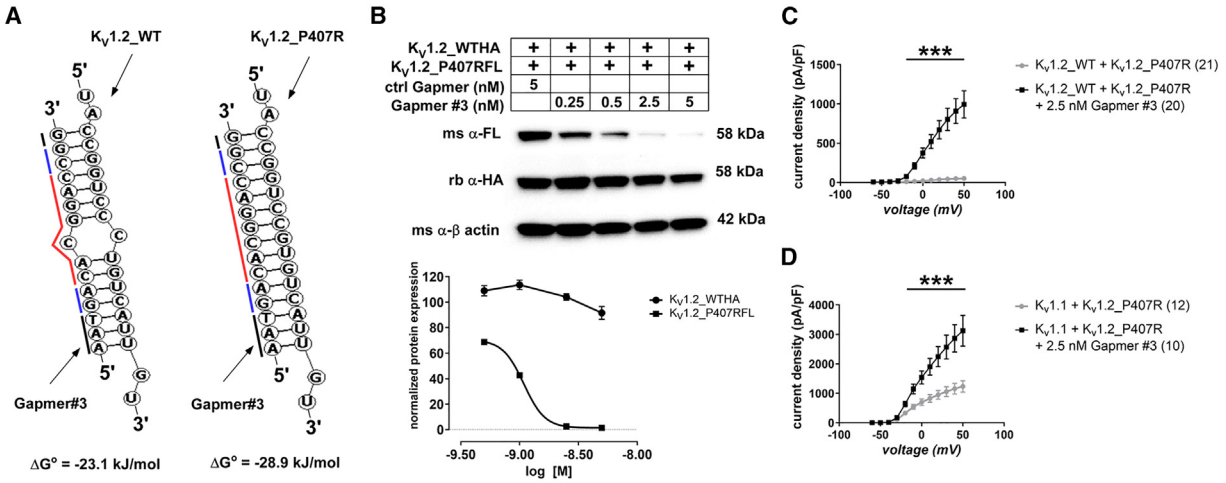

Figure 3. Gapmer#3 preferentially suppresses K_V1.2_P407R expression over the K_V1.2_WT and rescues K_V1.2 and K_V1.1 current density

(A) Structure prediction of the DNA-RNA complex between the Gapmer#3 and WT or P407R mRNA with the software RNA structure. The red regions indicate the unmodified nucleotides, locked nucleic acids are highlighted in blue and nucleotides with 2′-O-Methoxyethyl modification are highlighted with black line. The phosphodiester bonds are replaced with phosphorothioate linkage. The predicted Gibbs free energies are shown for respective structures. (B) Western blot showed the Gapmer#3 preferentially suppressed the expression of K_V1.2_P407R as compared with K_V1.2_WT protein. Top, the cells were transfected with HA-tagged WT and FLAG(FL)-tagged P407R with control Gapmer or Gapmer#3 with increasing concentrations as indicated. Middle, the intensities of HA-tagged WT and FLAG-tagged P407R bands were first normalized against the β-actin of respective sample and subsequently normalized against the cells transfected with control (ctrl) Gapmer to calculate the normalized expression. Bottom, dose-response curve of the effect of increasing concentrations of Gapmer#3 on the expression of WT and P407R protein. The data were fit with Y = Bottom + (Top-Bottom)/(1 + 10^((LogIC50-X)*HillSlope)). IC_{50} for P407R protein = 1.09 nM IC_{50} for WT is undetermined. (C) and (D) 2.5 nM Gapmer#3 rescued the K_V1.2_WT and K_V1.1 current density in cells co-transfected with K_V1.2_P407R. The number of cells recorded is indicated by the numbers in parentheses. Data for K_V1.2_WT + K_V1.2_P407R and K_V1.1+K_V1.2_P407R were reproduced from Figure 2 for comparison. ***$p < 0.001$. The data presented are mean ± SEM. Statistical significance was tested using unpaired Student's t test (2-tails).

(1995.31 ± 127.04 ms*mV) compared with WT (422.32 ± 23.98 ms*mV) or control neurons (410.20 ± 10.75 ms*mV) (Figures S5A and S5B). In addition, WT neurons displayed narrower APD_{50}, and higher AP frequency with injection of increasingly more positive currents (Figures S5C and S5D). This is potentially associated with stronger outward potassium currents in Kv1.2_WT expressing neurons (Figures S5G, S5H, and S5J), which supports more efficient repolarization of action potential and faster recovery from inactivation for sodium channels, thus allowing more frequent firing of AP upon depolarization. On the other hand, reduced outward potassium currents in Kv1.2_P407R (Figures S5G, S5I, and S5K) lead to broader APD_{50}. The AP frequency of Kv1.2_P407R neurons did not differ significantly from that of control neurons (Figure S5E). Curiously, WT neurons displayed lower rheobase, which was defined as the minimal current injection required to evoke action potential as compared with either control or P407R neurons (Figure S5F).

The neurons were further monitored on day 10 post viral transduction. AP area and APD_{50} measured in P407R neurons remained significantly larger compared to control neurons, correlating with diminished outward currents (Figure 4). In comparison, the peak outward currents recorded from WT became comparable to control cells perhaps due to the developmental upregulation of voltage-gated potassium currents in the neurons which could have buffered the additional potassium conductance afforded by overexpression of K_V1.2_WT proteins. Although the action potential frequency of WT neurons no longer differed significantly from control neurons, slightly narrower APD_{50} and lower rheobase remained to be observed in WT neurons. Additional electrophysiological parameters including AP amplitude, resting membrane potential and input resistance compared among the three types of neurons are summarized in Figure S6.

As a further verification of pathogenicity of c.1220C>G mutations, we employed CRISPR-Cas9-mediated genome editing of H9 human embryonic stem cells. The genotypes of H9-control and Homo-KI hESC were identified by DNA sequencing (Figures 5A and 5B) and subsequently both cell lines were differentiated into cortical neurons. Patch-clamp recording detected similar phenotypes of EAD and significant broadening of AP specifically in Homo-KI as compared with the H9-control neurons. Correlatingly, the outward potassium currents were also significantly diminished in the Homo-KI as compared with control reminiscent of rat cortical neuron overexpressing the P407R proteins (Figure 5).

LNP-Gapmer#3 treatment leads to down-regulation of K_V1.2_P407R subunits and reverses the EAD and APD50 broadening in P407R neurons

Cell-based assay of primary neurons provides a fast and simple model to detect underlying perturbation of electrophysiological parameters

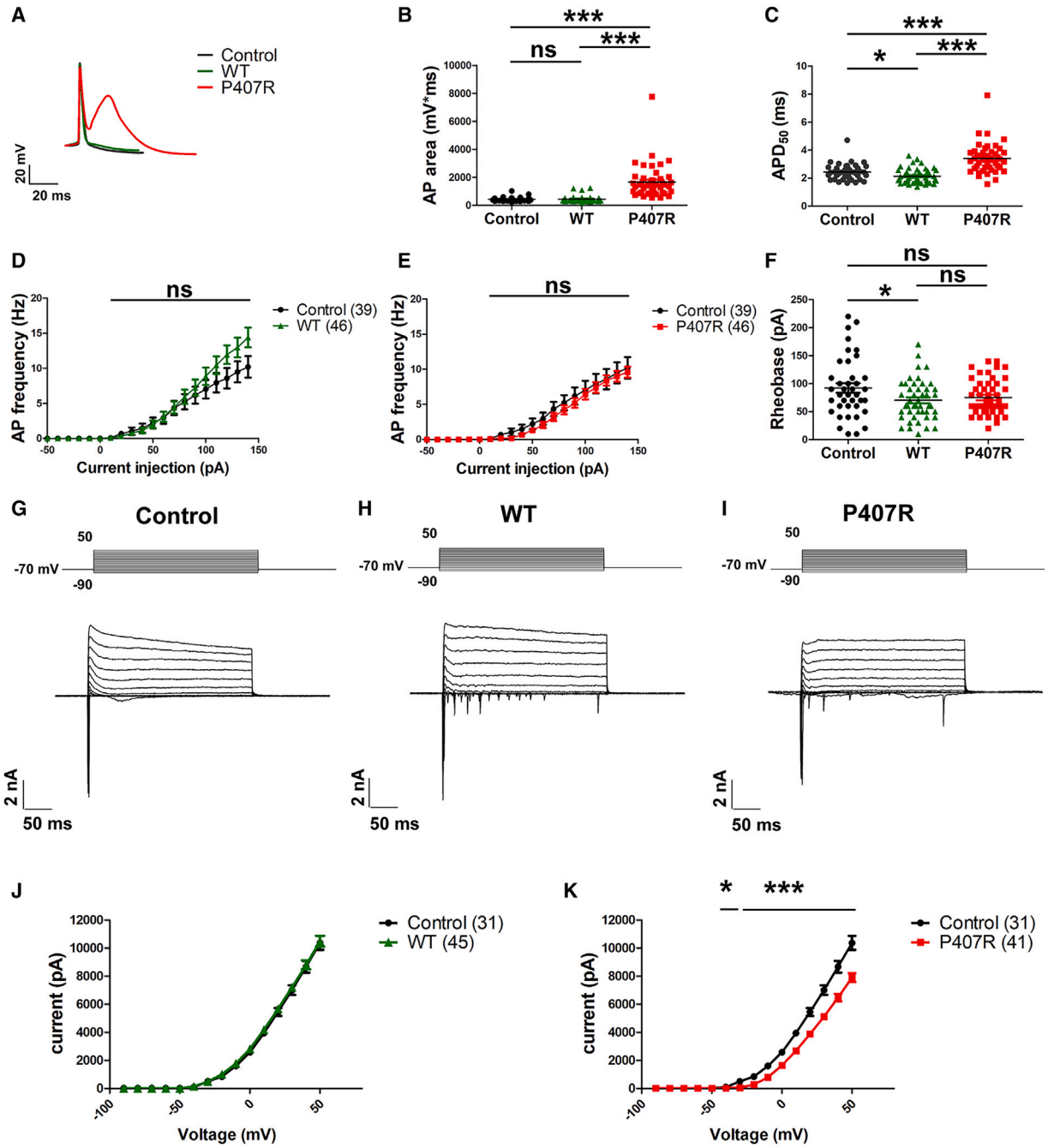

Figure 4. Overexpression of $K_V1.2$_P407R variants leads to early afterdepolarization (EAD), broadening of APD_{50} and diminishes outward current in cortical neurons upon viral transduction

(A) Overlayed exemplar action potential traces of control and $K_V1.2$_WT and P407R expressing neuron. (B and C) Data comparing AP area and 50% AP duration among the three types of cells. (D and E) Data comparing AP frequency with increasing current injection between WT and control neurons and P407R and control neurons respectively. The numbers of cells recorded are indicated by numbers in parentheses. (F) Data comparing rheobase among the three types of cells. (G–I) Exemplar traces of control, WT, and P407R neurons showing the voltage-sensitive currents evoked from a holding potential of −70 mV to different test potentials ranging from −90 mV to 50 mV with 10 mV increment. (J and K) Profile of outward potassium currents with comparison between WT and control neurons and P407R and control neurons, respectively. *$p < 0.05$ and ***$p < 0.001$; ns, nonsignificant. Statistical significance was tested using unpaired Student's t test (2-tails). The data presented are mean ± SEM.

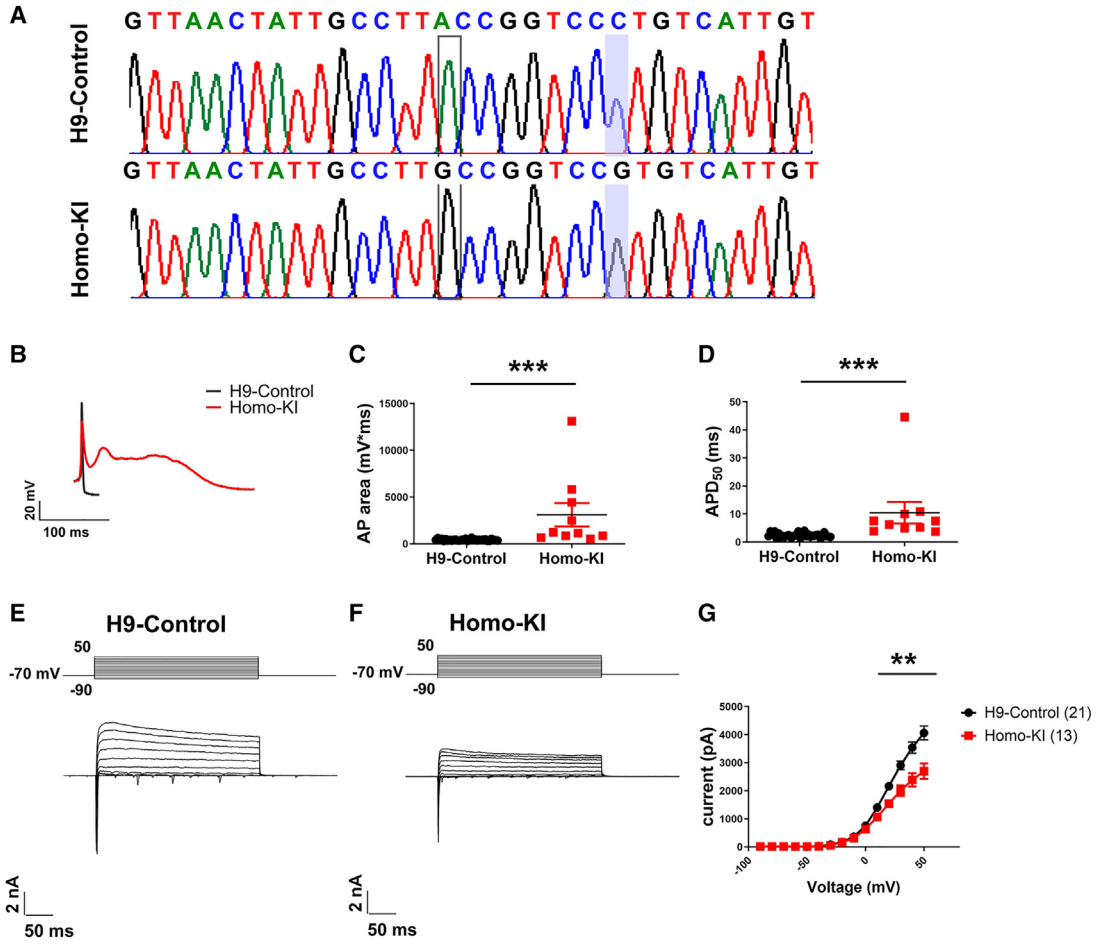

Figure 5. Homozygous knockin of *KCN2A* c.1220C>G in H9 hESC-derived cells results in early after depolarization (EAD) broadening of APD_{50} and diminished outward current

(A) Chromatograms showing the genotyping results of H9-control and Homo-KI cells. A silent mutation at c.1212A>G (highlighted in open box) was introduced along with c.1220C>G (highlighted with translucent blue bar) in the Homo-KI cells to prevent further binding and digestion of Cas9 protein to the genome DNA. (B) Overlayed exemplar action potential traces of H9 control and Homo-KI cells. (C and D) Data comparing 5 AP area and 50% AP amplitude between the two cell types respectively. (E) and (F) Exemplar traces of H9-control and Homo-KI neurons showing the voltage-sensitive currents evoked from a holding potential of −70 mV to different test potentials ranging from −90 mV to 50 mV with 10 mV increment. (G) Profile of outward potassium currents with comparison between H9-control and Homo-KI neurons. The number of cells recorded is indicated by the numbers in parentheses. $^{**}p < 0.01$ and $^{***}p < 0.001$. Statistical significance was tested using unpaired Student's t test (2-tails). The data presented are mean ± SEM.

and evaluate the efficacy of mutation-targeting Gapmers. However, to overcome the low transfection efficiency usually experienced with neuronal culture, Gapmer#3 was encapsulated into lipid nanoparticle with siRNA Spark transfection kit (Precision Nanosystems) containing siRNA Spark Nanoparticle Mix. K_V1.2_WT- and K_V1.2_P407R-expressing neurons were treated with increasing doses of LNP-Gapmer#3 and harvested for western blot 10 days post-treatment. Conformingly, increasing concentrations of Gapmer#3 led to progressively stronger inhibition of K_V1.2_P407R protein expression, densitometry analysis showed that Gapmer#3 suppressed K_V1.2_P407R expression with IC_{50} of 48.6 nM (Figure 6A) while the expression of K_V1.2_WT was not significantly affected compared with untreated cells.

Subsequently, to facilitate visualization of the uptake of LNP, Gapmer#3 was also packaged with GenVoy Ionizable Lipid Mix (GenVoy-ILM) that contains a red fluorescence-labeled dye. Live cell images of green and red fluorescence signals revealed robust integration of LNP into the neurons (Figure 6B). Curiously, the green fluorescence signals in LNP-Gapmer#3-treated P407R neurons was strongly suppressed compared with untreated cells, while no significant change in the green fluorescence signal was observed for Gapmer#3-LNP-treated compared with untreated WT neurons. Given that the coding sequence encoding K_V1.2_P407R was transcribed along with downstream IRES and EGFP sequence in the same mRNA transcript, it is plausible that binding of Gapmer#3 to the upstream mRNA of K_V1.2_P407R triggered RNase H activity

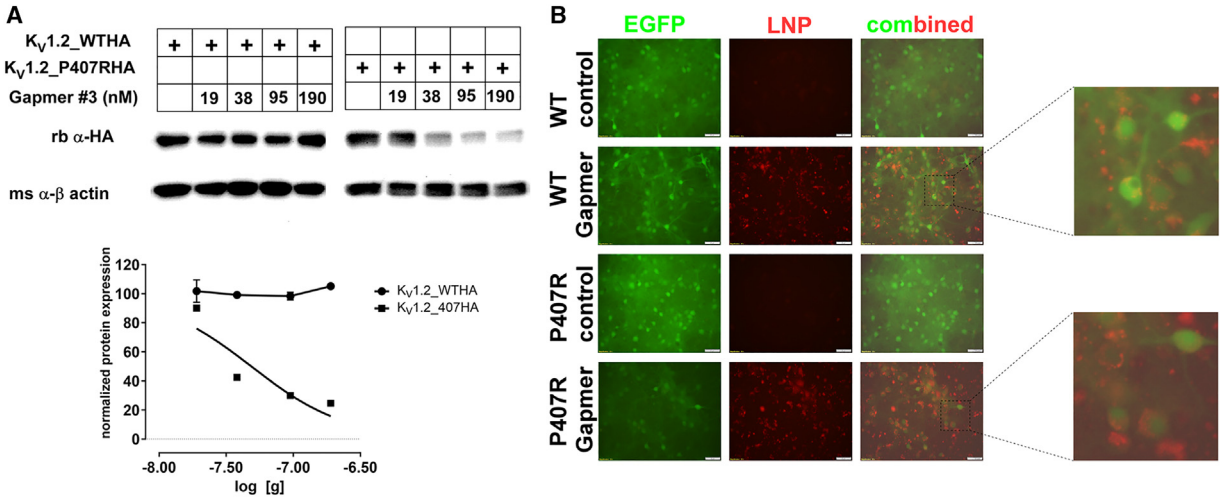

Figure 6. LNP-Gapmer#3 suppresses K_V1.2_P407R expression over the K_V1.2_WT in primary cortical neurons

(A) Western blot reporting the expression of K_V1.2_P407R as compared with K_V1.2_WT protein in cortical neurons treated with LNP-Gapmer#3. Top: the cortical neurons expressing HA-tagged K_V1.2_WT or K_V1.2_P407R were treated with increasing doses of LNP-Gapmer#3. Middle: the intensity of HA-tagged WT and P407R band were first normalized against the β-actin of respective sample and subsequently normalized against the control sample to calculate the normalized expression. Bottom: dose-response curve of the effect of increasing concentration of Gapmer#3 on the expression of WT and P407R protein. The data were fit with Y = 100/(1 + 10^((LogIC50-X)*HillSlope)). IC_{50} for P407R protein = 48.6 nM IC_{50} for WT is undetermined. The data presented are mean ± SEM. The experiment was carried out in duplicate. (B) Live imaging showing the decrease in EGFP fluorescence intensity selectively in K_V1.2_P407R expressing neurons treated with 190 nM Gapmer#3 packaged with GenVoy-ILM with a red fluorescence-labeled dye (Ex/Em: 644/665 nm). The areas in the boxes are enlarged to demonstrate the integration of red fluorescence-labeled dye as an indication of the uptake of LNP.

and led to the degradation of the entire mRNA (Figure S3A), thus suppressing EGFP expression as well. Conformingly, EGFP fluorescence remained robust in Gapmer#3-treated WT neurons, suggesting that the loss of EGFP fluorescence in P407R neurons was not due to an off-target effect of Gapmer#3 on EGFP mRNA. Similarly, Gapmer#3 packaged with GenVoy-ILM led to robust knockdown of Kv1.2_P407R expression in cortical neurons (Figure S7). The quality of LNP was analyzed with Malvern Zetasizer Nano ZS. The averaged diameter was 62.40 ± 1.28 nM, averaged PDI was 0.082 ± 0.043, and averaged Zeta potential was 0.36 ± 1.42 mV. The experiment was performed with three technical replicates.

The electrophysiological properties of the P407R and WT neurons were monitored 7 days and 10 days post LNP-Gapmer#3 treatment. On day 7, the APD_{50} of Gapmer#3-treated P407R neurons was significantly reduced, and the outward potassium current was significantly increased. However, EAD was still observed in a significant number of P407R neurons, and the AP area was not significantly different from untreated P407R neurons (Figure S8). In comparison, APD_{50}, AP area, and outward potassium currents was not significantly different between untreated and Gapmer#3-treated WT neurons (Figure S8). Progressively, on day 10, the EAD phenotype typical of the P407R neurons was completely abolished as indicated by the significantly reduced AP area (274.39 ± 30.28 ms*mV vs. 3213.33 ± 579.49 ms*mV, treated vs. untreated P407R neurons) (Figure 7). Correlatingly, APD_{50} was significantly reduced, and outward potassium currents were significantly increased in Gapmer#3-treated P407R neurons (Figure 7). In comparison, between untreated and Gapmer#3-treated WT neurons, no significant difference in APD_{50}, AP area, and outward potassium currents were observed (Figure 7). Additional electrophysiological parameters, including AP amplitude, resting membrane potential, and input resistance of the treated and untreated P407R and WT neurons are summarized in Figures S9 and S10.

DISCUSSION

In this current study, we have explored the therapeutic potential of Gapmer ASOs in targeting a novel dominant negative variant of K_V1.2 channel. Around 13 pathogenic variants have been characterized in the literature that are associated with epilepsy.[21–23] While the homozygous knockout of *KCNA2* in the mouse model is associated with enhanced seizure susceptibility and mortality at early postnatal age, heterozygous mice survive normally without developing seizures.[4] Thus, given patients harboring *KCNA2* mutations are usually heterozygous, a unifying mechanism could be proposed whereby K_V1.2 subunits exert dominant effect over the WT and possibly other K_V1 homologues via hetero-tetrameric assembly. Curiously, a nonsense mutation (NM_004974.3:c.637C>T); p.(Gln213*) was reported in a patient suffering from early-onset epileptic encephalopathy,[22] suggesting haploinsufficiency might be the another underlying pathogenic factor. However, our recent experiment suggested that such mutant mRNA could still yield a truncated protein variant containing N-terminal loop and S1 segment. Preliminary data suggested that such protein variant could also robustly inhibit K_V1.1 and K_V1.2 channel function (data not shown).

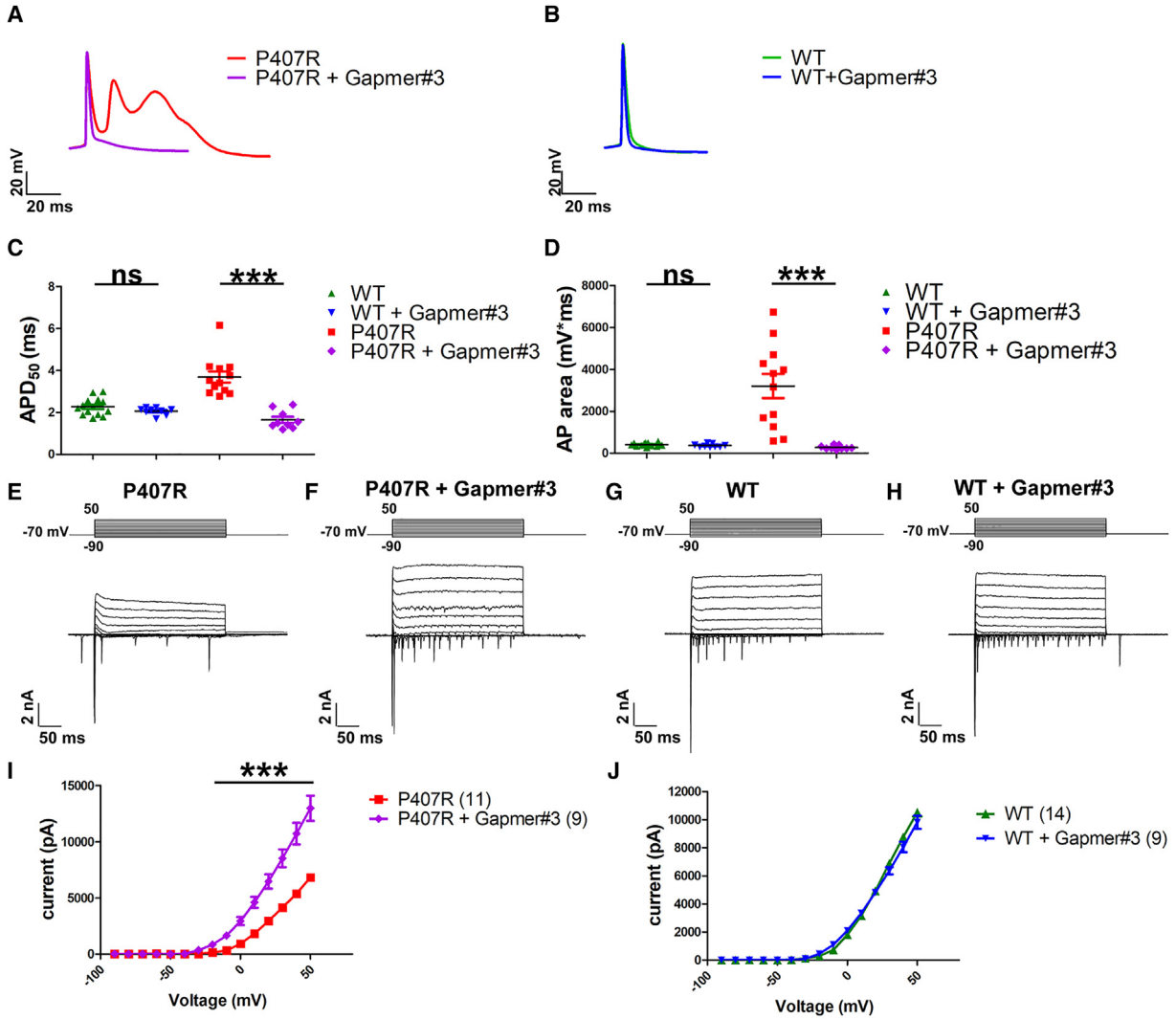

Figure 7. LNP-Gapmer#3 treatment on day 10 reduces APD_{50}, AP area, and increases outward potassium currents in $K_V1.2$_P407R expressing cortical neurons

(A) Overlayed exemplar action potential traces of $K_V1.2$_P407R and $K_V1.2$_P407R neurons treated with 190 nM of Gapmer#3. (B) Overlayed exemplar action potential traces of Kv1.2_WT and $K_V1.2$_WT neurons treated with 190 nM of Gapmer#3. (C and D) Data comparing 50% AP duration and AP area between WT and WT + Gapmer#3 or P407R and P407R + Gapmer#3. (E–H) Exemplar traces of WT, WT + Gapmer#3, P407R, and P407R + Gapmer#3 neuron showing the voltage-sensitive currents. (I and J) Profile of outward potassium current comparing WT and WT + Gapmer#3; and P407R and P407R + Gapmer#3 neurons, respectively. ***$p < 0.001$; ns, nonsignificant. Statistical significance was tested using unpaired Student's t test (2-tails). The data presented are mean ± SEM.

The K_V1 voltage-gated potassium channel subunit can form homo- or hetero-tetramers with random combinations. Hetero-tetramers may exhibit differing biophysical and pharmacological characteristics compared with homo-tetrameric channels.[9,24,25] Consequently, identifying small-molecule activators that fully address functional deficiencies in all channel complexes containing the toxic channel subunits might be complicated by the potential existence of diverse hetero-tetrameric channel structures. Additional challenges come from structural homology among the Shaker subfamily of voltage-gated potassium channels. Caution should also be excised to rule out the off-target effects of the small molecular drugs on the functional WT channel complexes. Of note, neuronal KCNQ/K_V7 potassium channel activator, Retigabine, was approved by the FDA in 2011 for the treatment of partial epilepsies and only to be withdrawn in 2017 because of unexpected ophthalmological and dermatological events.[26]

On the other hand, various gene-editing technologies are on the horizon that could potentially offer a cure to patients harboring pathogenic mutations. The FDA has recently approved the use of Casgevy, a therapy from Vertex Pharmaceuticals and CRISPR Therapeutics that employs CRISPR gene editing to treat the serious

blood disorder transfusion-dependent beta thalassemia. However, few gene-editing tools are available for diseases in the central nervous system. Base editing could not install transversion mutations such as c.1220C>G mutation in this case and postmitotic cells such as neurons are refractory toward genome editing via homology-directed repair (HDR).

While showing some promises, the most recently described prime editing technology remains rather inefficient in targeting neurons and comes with the significant risk of insertion and deletion mutations (indels). Employing the optimized v3em PE3-AAV9 system to introduce APOE Christchurch (APOE3 R136S) coding variant, a G-to-T transversion mutation, Davis et al. demonstrated that after 3 weeks of AAV injection, DNA editing efficiencies in bulk neocortical and hippocampal tissues for P1-injected mice were 12% with 5.0% indels and 14% with 3.1% indels, respectively. Injections at P3 resulted in even lower editing efficiency of 8.2% and 7.1% with 4.6% indels and 3.8% indels in the bulk neocortex and hippocampus tissues, respectively.[27]

Therefore, rather than targeting channel protein complexes or the genome, in the current study we have adopted the strategy of utilizing Gapmer ASO targeted to c.1220C>G mutation to selectively suppress expression of K_V1.2_P407R subunits. The remaining WT subunits could still form functional channels to support normal physiology. Significantly, co-transfection of c.1220C>G targeting Gapmer#3, K_V1.2_WT and P407R subunits revealed selective down-regulation of K_V1.2_P407R over the WT protein. Functionally, LNP-Gapmer#3 treatment reversed the broadening of action potentials, abrogated the EAD, and led to overall increase in potassium currents in K_V1.2_P407R-expressing neurons while electrophysiological properties of WT-expressing neurons were not largely altered by such treatment.

Ideally, future experiment entails derivation of hESC neurons from the proband and correction c.1220C>G mutation with CRISPR-Cas9 to yield isogenic control neurons. Treatment of patient-derived neurons with LNP-Gapmer#3 coupled with downstream RNA sequencing may be needed to fully assess the potency and off-target effects of Gapmer ASO.

From a broader perspective, while rapid development in DNA sequencing technology has allowed us to pinpoint disease-associated genetic variation, development of such "N of 1" therapies personalized for patients suffering from rare genetic disorders is not supported in the current drug development process due to the lack of measured benefit, regulatory restriction, and cost. This, therefore, represents an unmet clinical need.[28] In comparison with conventional small-molecule pharmaceuticals, which entails much larger, and often iterative, screening efforts followed by extensive medicinal chemistry optimization, the use of oligonucleotides is relatively straightforward and allows for design of precision and/or personalized medicine to selectively target any gene with minimal, or at least predictable, off-target effects. Mass vaccination of LNP-mRNA vaccine against COVID-19 has demonstrated the safety of *in vivo* delivery of nucleic acid therapeutics. Although this proposed intervention appears to benefit only a single patient at the moment, the principles derived from such endeavors could be generalized for treating other debilitating, drug-resistant neurological disorders associated with similar mutations. Moreover, the development of a pipeline from initial diagnosis in the clinic to preclinical experiment in the research labs to therapeutic development represents a translational collaborative effort among clinicians and basic researchers and helps develop research capability that could benefit patients suffering from debilitating genetic diseases in Singapore.

MATERIALS AND METHODS

Cloning of K_V1.1 and K_V1.2_WT and K_V1.2_P407R into expression vectors

The coding sequence of K_V1.1 and K_V1.2 were cloned from Human Brain, Whole Marathon-Ready cDNA Library (Takara Bio. 639300) into the pGEMT-easy vector (Progema) and confirmed by DNA sequencing. Subsequently, in the same vector, the c.1220C>G mutation was generated by circular mutagenesis. A hemagglutinin (HA) tag TACCCATACGATGTTCCAGATTACGCT or FLAG tag GACTACAAAGACGATGACGACAAG was engineered before the stop codon to facilitate the detection of the K_V1.1 and K_V1.2 proteins by western blot. The K_V1.1 was subcloned into the expression vector pIRES2-DsRed and K_V1.2_WT and K_V1.2_P407R coding sequences (cds) were subcloned into the pIRES2-DsRed and pIRES2-EGFP respectively to allow for identification by co-expression of reporter fluorescent proteins. For Lentivirus-mediated expression of EGFP alone (control), K_V1.2_WT or K_V1.2_P407R rat cortical neurons, the DNA sequence of IRES-EGFP or HA-tagged K_V1.2_WT and K_V1.2_P407R with downstream IRES-EGFP sequence in pIRES2-EGFP were cut with NheI and BsrGI restriction enzyme (NEB) subcloned into LentiCRISPRv2GFP (Addgene; plasmid #322457; RRID: Addgene_322457) replacing the Cas9-P2A-EGFP cassettes using the XbaI and BsrGI sites.

Cell culture and transfection

HEK293FT cells were cultured in Dulbecco's modified Eagle's medium (DMEM) supplemented with 10% fetal bovine serum (FBS) and 1% penicillin and streptomycin and maintained in 5% CO_2 incubator at 37°C. For transfection, cells are seeded on the petri dishes and grown overnight. Subsequently, the cells were either singly transfected with 2 μg of K_V1.2_WT, K_V1.1 or K_V1.2_P407R; or co-transfected with 2 μg of K_V1.2_WT and 2 μg K_V1.2_P407R, 2 μg of K_V1.2_WT and 2 μg K_V1.1, or 2 μg of K_V1.1 and 2 μg K_V1.2_P407R plasmids using lipofectamine 2000 (Inivtrogen Cat# 11668019). The transfected cells were incubated for 24 h in 5% CO_2 incubator at 37°C. The cells were split and seeded on poly-D lysine coverslips 1 day before recording.

Rat cortical neurons were obtained from P1 pups using the Papain Dissociation System (Worthington Cat# LK003150) and maintained in Neurobasal Plus Medium Thermo Fisher Scientific Cat# A358290

supplemented with B-27 Plus Supplement (Thermo Fisher Scientific Cat# A3582801). All procedures were in accordance with the Principles of Laboratory Animal Care and approved by the Institutional Animal Care and Use Committee.

Generation of *KCN2A* c.1220C>G cell line using CRISPR-Cas9 and neuronal differentiation

Human H9 ESC (Wicell) was cultured in mTeSR-1 plus medium (STEMCELL technologies) on tissue culture plates coated with Geltrex hESC qualified reduced growth factor basement membrane matrix (Thermo Fisher Scientific). For generating *KCN2A* c.1220C>G isogenic cell line, H9 hESC was digested with accutase (Thermo Fisher Scientific) to get a single cell suspension and subjected to electroporation. A total of 2×10^5 H9 single cells were incubated with 3 μg of Cas9 protein, 0.3 μg of gRNA mRNA (CACAATGACAGGGACCGGTAAGG), and 1 μL of 10 μM single-strand oligo donor (GTAGGCTATG GAGACATGGTTCCGACT ACCATTGGGGGAAAGATAGTGGG TTCCCTATGTGCGATTGCAGGTGTGTTAACTATTGCCTTGCC GGTCCGTGTCATTGTGTCCAATTTCAACTACTTCT; Cas9 protein, gRNA and oligo donor was synthesized by Integrated DNA Technology [IDT]) in 10 μL of buffer R. Electroporation was performed using the Neon Transfection System 10 μL Kit (Thermo Fisher Scientific), electroporation condition was optimized at 850 V, 30 ms, 2 pulses. The H9 cells were immediately plated onto Geltrex coated plates in mTesR-1 plus medium containing 10 μM ROCK inhibitor Y27632. Cells were counted after 48-h incubation, followed by serial dilution onto 96-well plates with a cell density of 1 cell per plate. After clonal expansion for 7–10 days, cells from individual wells were harvested, followed by genomic DNA extraction and PCR amplification of the target locus (forward primer: 5′- CTATGTGCGA TTGCAGGTGT -3′, reverse primer: 5′- CTTGCAAGTATTGGG CCTGT -3′). The PCR products were then cleaned and analyzed by Sanger sequencing.

For neural induction, H9 ES cells and isogenic cell lines were harvested using a scraper and cultured in suspension as embryoid bodies (EBs) for 8 days in StemPro defined medium (Thermo Fisher Scientific) minus FGF2. EBs were then be cultured for an additional 2–3 days in suspension in neural induction medium containing DMEM/F12 with Glutamax, NEAA, N2, and FGF2 (20 ng/mL) prior to attachment on cell culture plates coated with Geltrex. Neural rosettes were formed 2–3 days after adherent, and were isolated manually using a stretched glass Pasteur pipette and placed in fresh culture dishes. The rosettes were dissociated into single cells using accutase and replated onto culture dishes to obtain a homogeneous population of neural progenitor cells (NPCs). The NPCs were expanded in Neurobasal media containing NEAA, 2 mM glutamine, B27, and FGF2 (20 ng/mL). To induced cortical neuron, NPCs were cultured in Neurobasal medium supplemented with NEAA, L-glutamine (2 mM), B27, brain-derived neurotrophic factor (BDNF), and glial cell-derived neurotrophic factor (GDNF) (20 ng/mL of each), ascorbic acid (200 μM), and cAMP (1 mM) for 4 weeks on plates pre-coated with poly-L-ornithine (50 μg/mL, Sigma) and laminin (5 μg/mL, Sigma).

Whole-cell patch-clamp recordings and data analysis

Transfected HEK293FT cells were recorded with external solution containing (in mM): 125 NaCl, 2.5 KCl, 25 Na-gluconate, 1.0 $MgCl_2$, 1.8 $CaCl_2$, 10 HEPES, and 11.1 glucose, adjusted to pH 7.4 with NaOH. The cortical neurons were recorded with external solution containing (in mM): 10 glucose, 125 NaCl, 25 $NaHCO_3$, 1.25 $NaH_2PO_4.2H_2O$, 2.5 KCl, 1.8 $CaCl_2$, 1 $MgCl_2$, pH 7.4 (300–310 mOsm). Same internal solution (pipette solution) containing (in mM) 130 K-gluconate, 10 KCl, 5 EGTA, 10 HEPES, 1 $MgCl_2$, 0.5 Na_3GTP, 4 Mg-ATP, and 10 Na-phosphocreatine pH 7.4 (adjusted with KOH) was used for both transfected HEK293FT cells and cultured neurons. The cells were recorded with Axopatch 200B or multiclamp 700B amplifier (Molecular Device), low-pass filtered at 1 kHz and the series resistance was typically <5 MΩ after >80% compensation. The P/4 protocol was used to subtract online the leak and capacitive transients.

Third generation Lentivirus production

One day before transfection, 15×10^6 HEK293 cells were seeded into a 15-cm cell culture dish and grown into a confluency of 70%–90%. Polyethylenimine (PEI) was diluted in 2 mL of DMEM in a 1:3 DNA to PEI ratio and was incubated for 8–10 min at room temperature. Five micrograms of pMDL/pRRE (Addgene; plasmid #12251; RRID: Addgene_12251), 2.5 μg of pRSV-rev (Addgene; plasmid #12253; RRID:Addgene_12253), 2.5 μg of pMD2.G plasmids (Addgene; plasmid #12259; RRID:Addgene_12259), and 10 μg of transfer plasmids were diluted in 2 mL of DMEM. PEI was subsequently added, and the mixture was incubated for 20 min at room temperature before adding to 8 mL in DMEM supplemented with 3% FBS. The resultant mixture was subsequently added to the cells. Four to 6 h post transfection, the media was replaced with 20 mL of DMEM/F12. Supernatant was collected 24 h later, centrifuged at $1{,}000 \times g$ for 5 min, and was subsequently passed through a 0.45-μm Minisart syringe filter. Primary cortical neurons were infected 1 day post plating.

Western blot to detect expression of $K_V1.1$ and $K_V1.2$ proteins

Transfected HEK293FT cells or neurons were lysed with RIPA lysis buffer at 4°C. RIPA buffer consists of 150 mM sodium chloride, 0.1% Trion X-100, 0.5% sodium deoxycholate, 0.1% SDS, and 50 mM Tris, pH 8.0 supplemented with Mini, EDTA-free Protease Inhibitor Cocktail (Roche). Mouse (ms) anti-FLAG antibody (Sigma-Aldrich, Cat# F1804), rabbit (rb) anti-HA antibody (Sigma-Aldrich, Cat# H6908), and Rb anti-Kv1.1 Antibody (Alomone APC-009) was used in dilution of 1:1,000 and β-actin was stained with anti-β-actin (Sigma-Aldrich, A2228) antibody in the dilution of 1:10,000 as loading control.

Surface biotinylation assay

The surface biotinylation assay was performed with Pierce Cell Surface Biotinylation and Isolation Kit (Thermo Fisher Scientific, A44390). Briefly, 1.5 μg of HA-tagged $K_V1.2$_WT and $K_V1.2$_P407R plasmids were transfected into 3×10^5 HEK293FT cells cultured on six-well plates. Forty-eight hours post transfection, the cells were labeled with

EZ-Link Sulfo-NHS-SS-Biotin and subsequently lysed with 300 μL 1 mL NP40 buffer containing 150 mM sodium chloride 1.0% Triton X-100 and 50 mM Tris, pH 8.0 supplemented with Mini, EDTA-free Protease Inhibitor Cocktail (Roche). Thirty microliters of the clarified lysate was saved as total lysate while the remaining lysate was treated to 50 μL of NeutrAvidin Agarose beads to enrich for biotin-labeled surface fraction. The beads were subsequently washed four times with 1 mL NP40 denatured at 95°C with 60 μL of NP40 buffer supplemented with 6× loading buffer prior to SDS-PAGE and western blot. Transferrin receptor TFR was used as a loading control for surface protein detected with TFR antibody (Thermo Fisher Scientific, 136800) at 1:1000 dilution.

Design of Gapmer ASO and packaging of lipid nanoparticles for neuronal delivery

The following Gapmer ASOs (Gapmer#3) were ordered from IDT. The sequence for control Gapmer is 5′-CCTATAGGACTATCCAGGAA-3′ and the sequence for K_V1.2_P407R selective Gapmer (Gapmer#3) is 5′-AAT**GA**CACGGAC**CG**G-3′. The nucleotides contain the following modifications: 2′-MOE modifications and **locked nucleotides** that contain a methylene bridge between the 2′ oxygen and 4′ carbon of the pentose ring. A phosphorothioate linkage backbone was used to enhance nuclease resistance. Gapmer#3 was packaged into lipid nanoparticles (LNPs) with a small interfering RNA (siRNA) Spark transfection kit (Precision Nanosystems) containing siRNA Spark Nanoparticle Mix in stock concentration of 100 μg/mL. To facilitate the visualization of the uptake of LNP, the Gapmer#3 was also packaged with GenVoy Ionizable Lipid Mix (GenVoy-ILM) with a red fluorescence-labeled dye (Ex/Em: 644/665 nm) (Precision Nanosystems) in the same concentration. The cortical neurons cultured in a 24-well plate were treated on days *in vitro* (DIV) 7 and harvested on DIV17 for western blot. Recombinant Human APOE4 was first added to the neurons to a final concentration of 1 μg/mL media. Increasing doses of LNP packaged Gapmer#3, 19 nM (0.1 μg/mL), 38 nM (0.2 μg/mL), 95 nM (0.5 μg/mL), and 190 nM (1 μg/mL) were subsequently added to the cells. For electrophysiological recordings, the neurons were treated with 190 nM (1 μg/mL) Gapmer#3 on DIV4 and used for patch-clamp recording on DIV11 and DIV14, respectively.

DATA AND CODE AVAILABILITY

The data that support the findings of this study are available on request from the corresponding author (H.H.).

ACKNOWLEDGMENTS

The work has been supported by Singapore MOE AcRF Tier 1 grant (NUHSRO/2021/059/T1/Seed-Mar/02), MOE AcRF Tier 2 grant (MOE-T2EP30221-0018) and Singapore MOH Open Fund Large Collaborative Grant (MOH-OFLCG18May-0002).

AUTHOR CONTRIBUTIONS

H.H. conceptualized, designed, and performed the experiment. D.R.M. and E.K.T. performed genome editing of the hESC cell line, clonal selection, and neuronal differentiation. D.Y. performed the electrophysiology recording. T.W.S. conceptualized the experiment and provided intellectual input. S.J.N. and J.J.E.C. packaged Lentivirus. D.W.S.C., A.S.F.N., H.L.C., and D.L.M.G. provided clinical data to the manuscript.

DECLARATION OF INTERESTS

The authors declare no competing interests.

SUPPLEMENTAL INFORMATION

Supplemental information can be found online at https://doi.org/10.1016/j.omtn.2024.102316.

REFERENCES

1. Guerrini, R., Balestrini, S., Wirrell, E.C., and Walker, M.C. (2021). Monogenic Epilepsies: Disease Mechanisms, Clinical Phenotypes, and Targeted Therapies. Neurology *97*, 817–831.
2. Richards, S., Aziz, N., Bale, S., Bick, D., Das, S., Gastier-Foster, J., Grody, W.W., Hegde, M., Lyon, E., Spector, E., et al. (2015). Standards and guidelines for the interpretation of sequence variants: a joint consensus recommendation of the American College of Medical Genetics and Genomics and the Association for Molecular Pathology. Genet. Med. *17*, 405–424.
3. Döring, J.H., Schröter, J., Jüngling, J., Biskup, S., Klotz, K.A., Bast, T., Dietel, T., Korenke, G.C., Christoph, S., Brennenstuhl, H., et al. (2021). Refining Genotypes and Phenotypes in KCNA2-Related Neurological Disorders. Int. J. Mol. Sci. *22*, 2824.
4. Brew, H.M., Gittelman, J.X., Silverstein, R.S., Hanks, T.D., Demas, V.P., Robinson, L.C., Robbins, C.A., McKee-Johnson, J., Chiu, S.Y., Messing, A., and Tempel, B.L. (2007). Seizures and reduced life span in mice lacking the potassium channel subunit Kv1.2, but hypoexcitability and enlarged Kv1 currents in auditory neurons. J. Neurophysiol. *98*, 1501–1525.
5. Robbins, C.A., and Tempel, B.L. (2012). Kv1.1 and Kv1.2: similar channels, different seizure models. Epilepsia *53*, 134–141.
6. London, B., Wang, D.W., Hill, J.A., and Bennett, P.B. (1998). The transient outward current in mice lacking the potassium channel gene Kv1.4. J. Physiol. *509*, 171–182.
7. Feria Pliego, J.A., and Pedroarena, C.M. (2020). Kv1 potassium channels control action potential firing of putative GABAergic deep cerebellar nuclear neurons. Sci. Rep. *10*, 6954.
8. Al-Sabi, A., Shamotienko, O., Dhochartaigh, S.N., Muniyappa, N., Le Berre, M., Shaban, H., Wang, J., Sack, J.T., and Dolly, J.O. (2010). Arrangement of Kv1 alpha subunits dictates sensitivity to tetraethylammonium. J. Gen. Physiol. *136*, 273–282.
9. Köhling, R., and Wolfart, J. (2016). Potassium Channels in Epilepsy. Cold Spring Harb Perspect Med *6*, a022871.
10. Roberts, T.C., Langer, R., and Wood, M.J.A. (2020). Advances in oligonucleotide drug delivery. Nat. Rev. Drug Discov. *19*, 673–694.
11. Carroll, J.B., Warby, S.C., Southwell, A.L., Doty, C.N., Greenlee, S., Skotte, N., Hung, G., Bennett, C.F., Freier, S.M., and Hayden, M.R. (2011). Potent and selective antisense oligonucleotides targeting single-nucleotide polymorphisms in the Huntington disease gene/allele-specific silencing of mutant huntingtin. Mol. Ther. *19*, 2178–2185.
12. Southwell, A.L., Skotte, N.H., Kordasiewicz, H.B., Østergaard, M.E., Watt, A.T., Carroll, J.B., Doty, C.N., Villanueva, E.B., Petoukhov, E., Vaid, K., et al. (2014). In vivo evaluation of candidate allele-specific mutant huntingtin gene silencing antisense oligonucleotides. Mol. Ther. *22*, 2093–2106.
13. You, Y., Moreira, B.G., Behlke, M.A., and Owczarzy, R. (2006). Design of LNA probes that improve mismatch discrimination. Nucleic Acids Res. *34*, e60.
14. Labro, A.J., Raes, A.L., Bellens, I., Ottschytsch, N., and Snyders, D.J. (2003). Gating of shaker-type channels requires the flexibility of S6 caused by prolines. J. Biol. Chem. *278*, 50724–50731.
15. Tieleman, D.P., Shrivastava, I.H., Ulmschneider, M.R., and Sansom, M.S. (2001). Proline-induced hinges in transmembrane helices: possible roles in ion channel gating. Proteins *44*, 63–72.
16. Long, S.B., Campbell, E.B., and MacKinnon, R. (2005). Mammalian Shaker Kv1.2 potassium channel- beta subunit complex. https://doi.org/10.2210/pdb.2A79/pdb.
17. Mathews, D.H. (2006). RNA secondary structure analysis using RNAstructure. Curr. Protoc. Bioinformatics *12*, Unit–12.16.

18. Johnston, J., Forsythe, I.D., and Kopp-Scheinpflug, C. (2010). Going native: voltage-gated potassium channels controlling neuronal excitability. J. Physiol. *588*, 3187–3200.

19. Yue, C., and Yaari, Y. (2004). KCNQ/M channels control spike afterdepolarization and burst generation in hippocampal neurons. J. Neurosci. *24*, 4614–4624.

20. Metz, A.E., Spruston, N., and Martina, M. (2007). Dendritic D-type potassium currents inhibit the spike afterdepolarization in rat hippocampal CA1 pyramidal neurons. J. Physiol. *581*, 175–187.

21. Imbrici, P., Conte, E., Blunck, R., Stregapede, F., Liantonio, A., Tosi, M., D'Adamo, M.C., De Luca, A., Brankovic, V., and Zanni, G. (2021). A Novel KCNA2 Variant in a Patient with Non-Progressive Congenital Ataxia and Epilepsy: Functional Characterization and Sensitivity to 4-Aminopyridine. Int. J. Mol. Sci. *22*, 9913.

22. Masnada, S., Hedrich, U.B.S., Gardella, E., Schubert, J., Kaiwar, C., Klee, E.W., Lanpher, B.C., Gavrilova, R.H., Synofzik, M., Bast, T., et al. (2017). Clinical spectrum and genotype-phenotype associations of KCNA2-related encephalopathies. Brain *140*, 2337–2354.

23. Nilsson, M., Lindström, S.H., Kaneko, M., Wang, K., Minguez-Viñas, T., Angelini, M., Steccanella, F., Holder, D., Ottolia, M., Olcese, R., and Pantazis, A. (2022). An epilepsy-associated K(V)1.2 charge-transfer-center mutation impairs K(V)1.2 and K(V)1.4 trafficking. Proc. Natl. Acad. Sci. USA *119*, e2113675119.

24. Coleman, S.K., Newcombe, J., Pryke, J., and Dolly, J.O. (1999). Subunit composition of Kv1 channels in human CNS. J. Neurochem. *73*, 849–858.

25. Ruppersberg, J.P., Schröter, K.H., Sakmann, B., Stocker, M., Sewing, S., and Pongs, O. (1990). Heteromultimeric channels formed by rat brain potassium-channel proteins. Nature *345*, 535–537.

26. Brickel, N., Hewett, K., Rayner, K., McDonald, S., De'Ath, J., Daniluk, J., Joshi, K., Boll, M.C., Tiamkao, S., Vorobyeva, O., and Cooper, J. (2020). Safety of retigabine in adults with partial-onset seizures after long-term exposure: focus on unexpected ophthalmological and dermatological events. Epilepsy Behav. *102*, 106580.

27. Davis, J.R., Banskota, S., Levy, J.M., Newby, G.A., Wang, X., Anzalone, A.V., Nelson, A.T., Chen, P.J., Hennes, A.D., An, M., et al. (2024). Efficient prime editing in mouse brain, liver and heart with dual AAVs. Nat. Biotechnol. *42*, 253–264.

28. Aartsma-Rus, A. (2021). N of 1' therapies need a better model. Nat. Med. *27*, 939.